ingegneria sismica
International Journal of Earthquake Engineering
Anno XLIII - Num. 1 - 2026

Innovation of Gas Unit Inspection Mode and Construction of Cockpit Platform under the Perspective of Smart Power Plant

Jiacheng Peng[1,*]

[1] Guoneng Guohua (Beijing) Gas Thermoelectric Co., Ltd., Beijing, 100024, China

SUMMARY: *Selecting the gas-steam hybrid cycle as the research target, the mathematical model of the unit and the system is created. To compensate for the weaknesses of the BP neural network, the gravitational search method is employed to optimize the BP neural network, thus creating a GSA-BP gas unit condition monitoring and prediction model. The power station's operational data over a period of around one year was selected, and 2,732 effective samples were obtained as research materials. Tests show that the forecasting error of the gas turbine's output power can be steadily maintained below 0.5 MW, and the GSA-BP model is capable of accurately reflecting the characteristics of the unit under different loads. Based on the basic principles of the bidirectional RRT algorithm, the improved bidirectional RRT algorithm is proposed based on artificial potential field theory. The simulation test in the scenario of gas unit inspection shows that the improved bidirectional RRT algorithm performs better than the traditional RRT algorithm and bidirectional RRT algorithm in terms of optimal performance and planning speed. Finally, the intelligent inspection cockpit platform of gas units is developed. This intelligent inspection cockpit platform is of great significance to the transformation of the operating and maintenance shift mode and improving the automation level of operating and maintaining.*

KEYWORDS: *gas turbine; BP neural network; gravity algorithm; power prediction; two-way RRT algorithm*

1 Introduction

Nowadays, in the rapid development of society, energy has become an indispensable part of the development of human civilization. Nevertheless, fossil fuels, especially natural gas, remain responsible for over 80% of the global energy consumption needs, and they represent finite resources that make the expansion of conventional energy systems rather difficult [1, 2]. Therefore, constructing a new type of power system, improving the efficiency of natural gas utilization, and vigorously developing clean and efficient natural gas power generation technology is the necessary way to transform the energy structure [3, 4].

The gas-steam combined cycle power generation technology provides another efficient approach towards the creation of green energy technologies based mainly on natural gas. It demonstrates a set of considerable benefits, including low levels of greenhouse emissions, higher generation efficiency, flexibility in operation and shorter construction period and higher rates of investments return on investment. Thus, it can be considered suitable for the development of new power systems [5-9]. As mentioned above, the construction of the gas-steam combined cycle generating unit involves the installation of multiple units, including the

*pengjiacheng1980@163.com
https://doi.org/10.65102/is2026482
Published: 30 April, 2026

gas turbine that serves as the core equipment in terms of its importance for the whole plant. Its proper operation directly influences the safety and productivity of the plant itself [10-12]. Under normal operating conditions, air and natural gas are regularly supplied into the combustion chamber, mixed, combusted and converted into high temperature gases, which, after the turbine expansion, are converted into mechanical energy. This type of energy activates the process of compression and the process of generation of electricity starts [13-17].

It is because of the importance of the gas unit, but also because of the high price of the gas unit equipment, for its inspection and operation and maintenance is very necessary, which can not only significantly reduce the maintenance expenses of the power plant but also increase the life expectancy of the gas unit [18-20]. However, the traditional gas unit inspection is based on manual inspection and vibration monitoring system, the manual inspection time is longer, and the monitoring system is insufficient to capture and diagnose small defects, it is difficult to adapt to and meet the complex operating environment of the gas unit equipment and the data island effect [21-23]. The smart power plant, as the development direction of the power enterprise in the next decade, is based on the foundation of enterprise digitalization and informatization construction, which organically integrates the cloud platform, Internet of Things, robotics, artificial intelligence and other advanced technological means with the safety production and operation control of traditional electric power enterprises, so as to keep the power plant in a good operating state of high security, good economy, green environmental protection, and strong adaptability [24]. Based on this background, the innovation of gas unit inspection mode and the construction of inspection cockpit platform to realize the intelligent upgrade of gas unit.

In this study, the first task was to construct a state prediction model of the gas-steam co-generation unit, aiming at the understanding of the working features of the entire unit. Next, a model of the gas unit status identification was built using the combination of the GSA algorithm and the BP neural network. Through the selected characteristic parameters, then using SIS to observe the operation of the unit, determine the time range of the data samples, and complete the optimization of the network parameters, set up experiments to analyze the performance of GSA-BP. Besides, a new approach to UAV-assisted gas unit inspection route planning based on the bidirectional RRT algorithm has been put forward. The novel algorithm has taken advantage of the artificial potential field theory to enhance the classical bidirectional RRT algorithm. The proposed method has been compared with the RRT algorithm and the traditional bidirectional RRT algorithm. Finally, a gas unit intelligent inspection cockpit platform is constructed to improve the intelligence and automation level of gas unit operation and maintenance.

2 Mathematical modeling of gas units

2.1 Gas-fired combined cycle units

Gas-steam combined cycle unit configuration includes two main components: gas turbine cycle that operates as an open cycle and steam power cycle as a closed cycle. Steam power cycle utilizes the exhaust waste heat from the gas turbine cycle to increase the efficiency of the entire unit. A usual configuration includes one gas turbine, one steam turbine, one waste heat boiler, and two generators. The unit features a two-shaft scheme with 3,000 revolutions per minute rated speed. Natural circulation waste heat boiler with non-compensated steam is used here, while the steam turbine represents double cylinder construction when both high-pressure and low-pressure steam enter the turbine to perform work. During normal operation, turbine control valve is opened completely and the unit works at sliding pressure. In its turn, the turbine does not participate in load control, and load control is performed by the gas turbine.

2.2 Mathematical modeling of the system

Figure 1 shows the mathematical model of the traditional gas-steam combined cycle unit. The model uses some simplifications for the unit, thus lowering the overall complexity of the unit. The main elements of the model are: fuel supply module, compressor inlet guide vane (IGV) module, exhaust gas temperature module, gas turbine output module, waste heat boiler and turbine module, and speed load control module. Gas turbine air flow (W), gas turbine fuel flow (W_F), gas turbine heat power (Q_{GT}), gas turbine exhaust heat (Q_E), gas turbine output power (P_{GT}) and steam turbine Output power (P_{ST}) and other parameters are normalized by rated operating conditions.

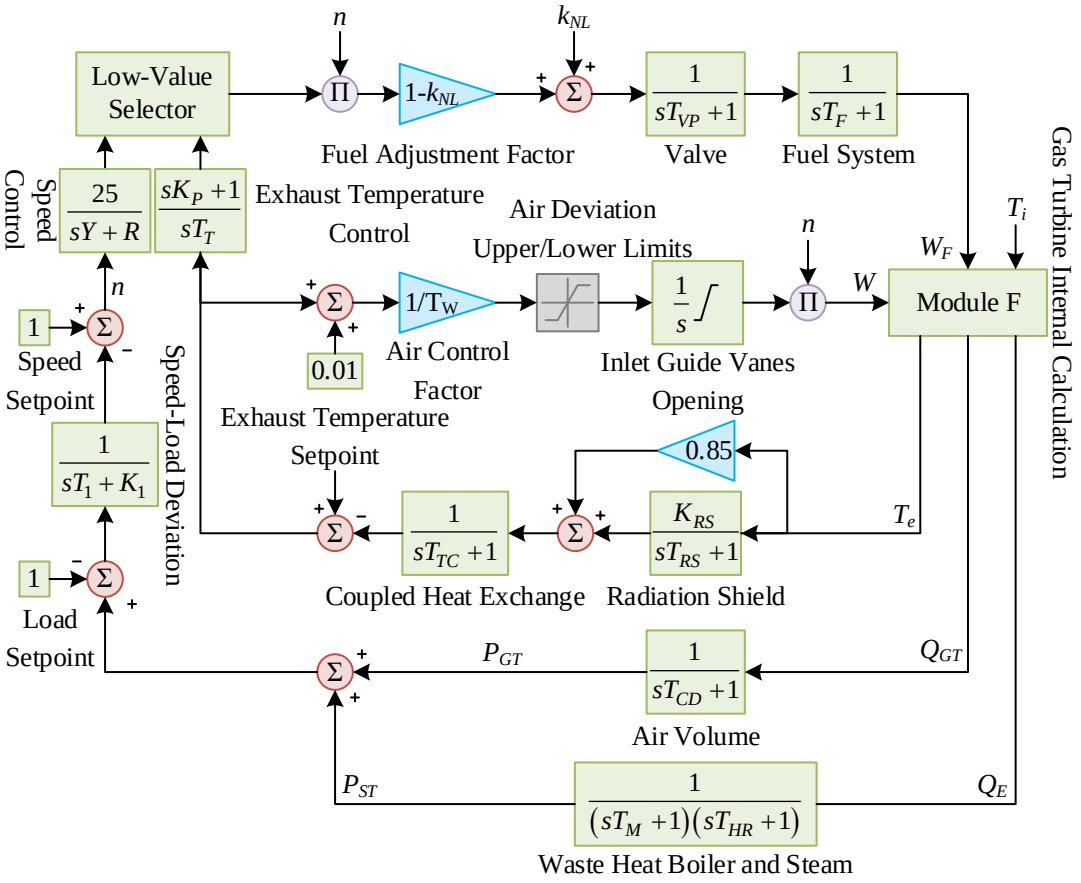

Figure 1: Simplified Mathematical Model of Gas-Steam Combined Cycle Unit

The basic working principle of the control mechanism of the model is described below. Both the speed signal and the exhaust gas temperature signal are processed using the low value selector, and then fed into the fuel supply module. The fuel supply module provides fuel flow signals to the gas turbine output module, which contains the fuel conditioning coefficients, valves and fuel system. The inlet guide vane module provides air flow signals for the gas turbine output module, which contains air control coefficients, air deviation upper and lower limits and inlet guide vane openings. The exhaust temperature module includes the radiant shield and coupled heat exchanger, provides the exhaust temperature deviation signal for the inlet guide vane module and outputs the exhaust temperature signal to the low value selector through the exhaust temperature control link. The gas turbine output module includes the gas turbine internal calculation module F and air volume link. There are three inputs in the module F

from the inlet guide vane module, the fuel supply module and the given ambient temperature, and after internal calculation, the three outputs are output to the exhaust temperature module, the air volume block, waste heat boiler, and turbine module are used to process signals individually. The thermal power of gas turbine flows through the air volume block to acquire output power of gas turbine, whereas the exhaust heat flows through the waste heat boiler and turbine module to produce output power of steam turbine. Rotational speed load module acquires output power of both gas turbine and steam turbine and processes speed signal to the low value selector.

The calculation formula within the module F is:

$$T_d = T_i\left(1+\frac{x-1}{\eta_c}\right) \tag{1}$$

where: T_d for the outlet temperature of the press, K; x for the ratio of the press import and export temperature; η_c for the press efficiency, generally take 0.85 ~ 0.9.

$$x = \left(\pi W\right)^{\frac{\gamma-1}{\gamma}} \tag{2}$$

where: π denotes the pressurizer pressure ratio; π denotes the ratio of specific heat capacity at constant pressure to specific heat capacity at constant volume.

$$T_f = T_d + \left(T_{f0} - T_{d0}\right)\frac{W_f}{W} \tag{3}$$

where: T_f denotes the turbine inlet temperature, K; Tf0T_{f0} Tf0 denotes the rated turbine inlet temperature, K; T_{d0} denotes the rated pressurizer outlet temperature, K.

$$T_e = T_f\left[1-\left(1-\frac{1}{x}\right)\eta_t\right] \tag{4}$$

where: T_e denotes the turbine exhaust temperature, K; T_f denotes the turbine inlet temperature, K; η_t denotes the gas turbine efficiency; the value adopted within this interval is generally taken to be equal to the compressor efficiency.

$$Q_{GT} = K_0\left[(T_f - T_e) - (T_d - T_i)\right]W \tag{5}$$

where: K_0 is the output coefficient of the gas turbine; T_d is the pressurizer outlet temperature, K; and T_i is the ambient temperature, K.

$$Q_E = K_1 T_e W \tag{6}$$

where: K_1 is the steam power cycle output coefficient.

In modeling the steam power cycle, the waste heat boiler and the turbine are regarded as inertial links without taking into consideration the dynamics of these components. In this case,

the accuracy of the model is bound to be reduced to some extent.

3 UAV-based gas unit condition inspection

3.1 Principles of GSA-BP

3.1.1 BP Neural Network

BP neural network modeling consists of two processes when training the network. These two processes include signal forwarding and error forwarding processes. Signal forwarding sends signals forward to the output from the hidden layer. The moment when the difference between the output and target results is too wide, error forwarding will take place. While doing so, the network's weights continue changing till they get optimized. The whole process repeats itself many times until the difference between the output and the desired results fulfills the stopping condition.

Given an input sample $x_1, x_2, \cdots, x_n$, the forward propagation process initializes the weights $w_1, w_2, \cdots, w_n$ and the threshold θ, and the input values of neurons in the hidden layer are then obtained by computing the samples against the initial weights and threshold, as shown in Equation (7):

$$u_j = \sum_{i=1}^{n} w_i x_i - \theta_j \tag{7}$$

When the model is a multi-layer implicit layer structure, the next layer of inputs is computed based on the current inputs, as shown in equation (8):

$$f(u_j) = \frac{1}{\left(+\exp\left(-u_j\right)\right)} \tag{8}$$

Output values across all layers are obtained through the above equation. The output value is labeled as ζ^*, and the discrepancy between this output value ζ^* and the desired value ζ is then computed, as given in Equation (9):

$$\delta = \sum_{i=1}^{n} \left(\zeta^* - \zeta\right)^2 \tag{9}$$

Based on the error δ, the weights w and threshold θ are adjusted accordingly, transferring corrections from the output layer back to the input layer. Through this iterative cycle of forward and backward propagation, the BP neural network model achieves the selection and optimization of parameters, bringing the difference between the final output value and the expected value within the required tolerance range, thereby completing the training of the model.

3.1.2 GSA Algorithm Flow

In the case of the gravitational search algorithm (GSA), all particles considered possess mass, and during the whole process, their movement occurs in the absence of any resistance force. Each particle will experience an attractive force from all other particles present in the space

towards the one possessing higher mass. This is because of the correlation that exists between the mass and fitness value of each particle; hence, the higher the fitness value, the larger the mass. As a result, particles with less mass slowly move towards the one having larger mass, leading to the discovery of the optimal point. The gravitational search algorithm entails the following procedure steps:

Step 1: Initialize the location and acceleration of all particles in the algorithm and provide the number of iterations and other related parameters.

Step 2: Determine the fitness value for each particle and calculate the gravitational constant based on the following equation:

$$G(t) = G_0 \times e^{-\alpha t/T} \tag{10}$$

where: $G(t)$ denotes the universal gravitational constant that varies with gravity; G_0 denotes the value of G at the initial moment t_0; T is the maximum number of iterations; t is the current time; and a is the acceleration of the particle.

Step 3: Calculate the mass of each particle from the computed fitness values using Eq. (11) and Eq. (12):

$$\begin{cases} m_i(t) = \dfrac{fit_i(t) - worst(t)}{best(t) - worst(t)} \\ M_i(t) = \dfrac{M_i(t)}{\sum_{j=1}^{N} M_j(t)} \end{cases} \tag{11}$$

$$\begin{cases} best(t) = \max\ fit(t) \\ best(t) = \min\ fit(t) \end{cases} \tag{12}$$

where $fit_i(t)$ denotes the adaptation value of the particle; $best(t)$ denotes the optimal solution in t moments; $worst(t)$ denotes the worst solution in t moments; and $m_i(t)$ normalizes to the adaptation value of the particle between $[0,1]$.

Step 4: And calculate the acceleration of each particle using Eq. (13) to Eq. (16):

$$F_{ij}^k(t) = G(t)\frac{M_{pi}(t) \times M_{aj}(t)}{R_{ij}(t) + \varepsilon}\left(x_j^k(t) - x_j^k(t)\right) \tag{13}$$

$$R_{ij}(t) = \left\| X_i(t), X_j(t) \right\|_2 \tag{14}$$

$$F_i^k(t) = \sum_{j=1, j\neq 1}^{N} rand_j F_{ij}^k(t) \tag{15}$$

$$\alpha_i^k = \frac{F_i^k(t)}{M_{ii}(t)} \tag{16}$$

where: ε denotes a very small constant; $M_{aj}(t)$ denotes the inertial mass of the acting object j; $R_{ij}(t)$ denotes the Euclidean distance between objects X_j; $F_i^k(t)$ is the force acting on the object; and $M_{ii}(t)$ is the inertial mass of the object.

Step 5: Calculate the velocity of each particle according to Eq. (17), and subsequently update the position of the particle:

$$\begin{cases} v_i^k(t+1) = randv_i^k(t) + \alpha_i^k(t) \\ x_i^k(t+1) = x_i^k(t) + v_i^k(t+1) \end{cases} \tag{17}$$

where: $v_i^k(t+1)$ and $x_i^k(t+1)$ are the velocity and position of the object after updating.

Step 6: If the termination condition is not satisfied, return to Step 2; otherwise, output the optimal solution of the algorithm.

The principle of neural network performance monitoring can be understood as follows: if the general approach of physical structure and modeling method is used, the modeling is difficult and not precise enough due to the complexity of the mechanism structure, the coupling between the parameters, and the difficulty of obtaining the physical parameters. Considering the dynamic system of the actual equipment as a black box, using the neural network algorithm, we don't need to care about the mechanism structure inside the black box, but only need to find the relevant characteristic parameters between the input and output of the black box, and through extensive training on normal operating data, the neural network model is capable of establishing the relationship between input and output data of equipment under normal conditions. A discrepancy will inevitably exist between the predicted output y_1 of the model and the actual measured output y_2, denoted as E. When the actual equipment state does not deviate considerably from the normal condition, E remains within a very small range. Once the equipment begins to exhibit performance degradation, a threshold value L is defined, and the system is considered to have developed an abnormality when $E > L$.

The flow chart of the condition monitoring system based on the GSA-BP neural network is shown in Fig. 2.

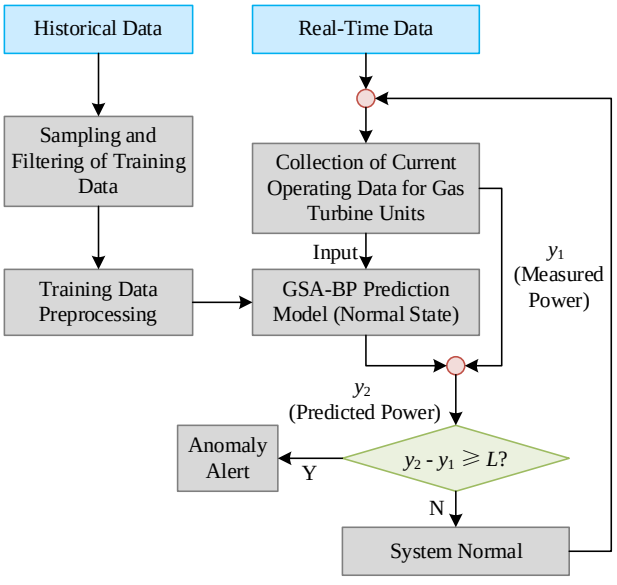

Figure 2: Power Prediction Model Flowchart

3.2 Data selection for the prediction model

3.2.1 Selection of feature parameters

Factors affecting gas turbine output work as well as exhaust temperature: ambient temperature, IGV opening, gas temperature, gas pressure, gas calorific value, and IGVM opening.

3.2.2 Anomaly Rejection

The first step is to preprocess the data and eliminate the abnormal data. Combined with the actual data analysis, this paper for the following data to be screened out:

(1) Measurement point data for the null value NULL, due to the sensor or communication process of data loss.

(2) A moment of measurement point data is greater than or less than the usual data by more than one order of magnitude, these data deviate from the normal data range, can be regarded as an isolated point, should be eliminated.

(3) The gas unit current is 0 or negative, 0 means that the gas unit has stopped working, which is not possible in the operating state of the unit.

3.2.3 Normalization

It is necessary to apply uniform normalization to both the input and output samples of the GSA-BP neural network. The normalization method used in this paper is the max-min algorithm, which aims to transform the data of each dimension (i.e., each row) in the dataset into the interval of $[-1,1]$ in order to eliminate the effects brought by the magnitude and the size of the values between the dimensional data. The formula is as follows:

$$p_1 = 2 * \frac{p - \min}{\max - \min} - 1 \tag{18}$$

where p is the original vector prior to normalization, p_1 is the output vector after normalization, and $\max$ and $\min$ are the maximum and minimum values respectively. It is worth noting that when an S-shaped function is chosen as the activation function of the neural network, the data should be normalized to the $[0,1]$ interval, given that its output value domain is $(0,1)$.

It is clear that once the training phase of the neural network is completed after data normalization, then the test data must also be normalized, and the max and min values used in the process should match those used when normalizing the training data. This is because the output data generated by the neural network itself is normalized data.

3.2.4 Data acquisition

By querying the gas unit operation of the SIS platform of the power plant, it can be learned that the gas unit 9 of the power plant started to operate on May 27, 2021, and has been operating continuously for about one year since then, and the unit operation time is the operation time of the gas engine system. After the shutdown and maintenance, the state of the gas engine system put into operation is the best period, and hence the data gathered during this period may be used for the training of the neural network. Therefore, this paper reasonably selects the actual operation data under different load conditions (300mw-600mw) within one month at the beginning of the unit's operation, and avoids centralized selection, and excludes obvious

anomalies, so that a total of 2,732 effective data samples are screened in the end. In this case, 2,428 sets of these data are used for training, while the other 304 sets of data are used as test data to test the training result of the neural network.

3.3 GSA-BP Neural Network Parameter Selection

3.3.1 GSA parameter selection

The significance of the gravitational constant G_0 is the coefficient of the particle step size in the algorithm, for different functions, the selection of this parameter is too large or too small may produce diametrically opposite effects due to the fact that the distribution of their optimal solutions and the size of the solution space are different. Therefore, after many simulation tests, $G_0 = 100$ is finally selected, which is also the most selected value by the original authors, including the related papers, and it makes the algorithm results more stable.

The decay coefficient α is also a variable in the formula for calculating the gravitational constant, and it can be seen that α represents the rate of decay of the gravitational coefficient, which is the same as other population optimization algorithms that use the decreasing step method to improve, and this factor in the gravitational algorithm ensures the fast convergence of the search for the optimum. If this parameter is chosen to be large, the rate of decreasing step size will become faster, resulting in the particles rapidly entering the local optimization search, this indicates that it combines global search performance and local search performance. As the objective of improving the BP algorithm in this paper does not necessarily require extremely good accuracy, while a better global search performance of GSA is preferred, α=10 is chosen.

3.3.2 Neural Network Parameter Selection

The first step is to determine the number of layers in the neural network. According to Kolmogorov's theorem, for any continuous mapping $F:[0,1]^{(n)} \to R^m$, a three-layer feed-forward neural network is adequate for its accurate approximation, implying that a three-layer network is adequate for meeting the approximation criteria of any nonlinear function. Thus, a three-layer network is chosen to construct the GSA-BP neural network model.

In respect of selecting the number of nodes in the hidden layer, the basic rationale behind the choice lies in the fact that applications of neural networks do not possess general applicability across various problems, and each particular problem requires separate analysis. Much research has been conducted on the automated determination of the number of nodes in the hidden layer. In this study, we adopt a step-by-step testing method, and its details are not presented again. The final number of nodes in the hidden layer is chosen to be 8.

3.4 Gas Turbine Unit Condition Inspection Results

Through data pre-screening, network architecture and transfer function determination, and choosing the learning algorithm, the learning rate is set to 0.01, the goal error is chosen to be 0.0001, and the maximum iteration number is set to 100. The process of the outer loop iteration is shown in Fig. 3. GSA-BP modifies the learning factors as well as the weights during training through the validation set, and eventually the accuracy starts to stabilize in the 90th iteration and stops at the 100th iteration.

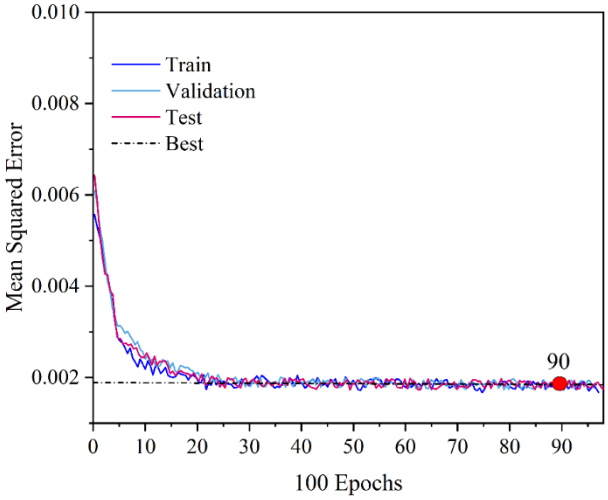

Figure 3: The Iteration Process of Gas Turbine GSA-BP

The fit of the training results is shown in Fig. 4. There is no clear evaluation standard for the GSA-BP fit, but the default fit is greater than 0.9, which indicates that the trained GSA-BP can predict the actual output well. From the figure, it can be seen that the predicted output closely fits the transfer function, which proves that the trained GSA-BP has been able to fit the mapping relationship between the data inputs and outputs well, and the fit of the training set, the validation set and the test set do not differ much, which proves that there is no overfitting in the training process.

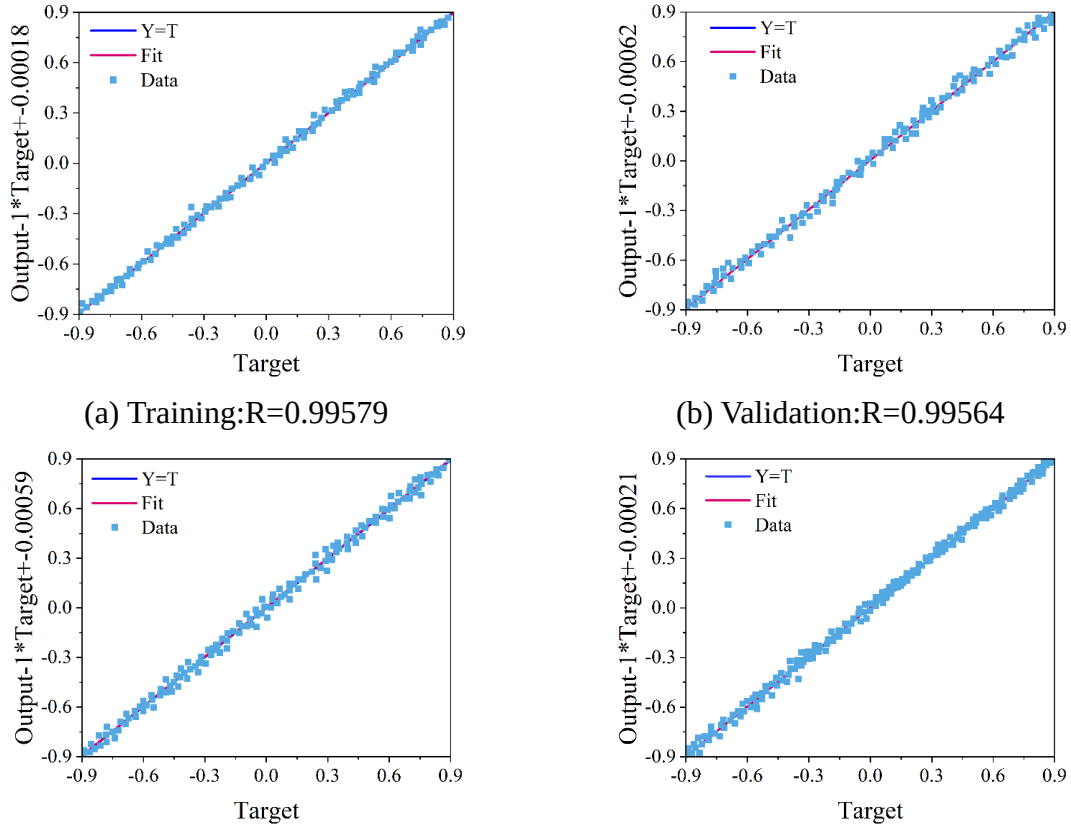

(a) Training:R=0.99579 (b) Validation:R=0.99564

(c) Test:R=0.99554 (d) All:R=0.99569

Figure 4: The fitting degree of the training results of gas turbine GSA-BP

The gas turbine output power training results and the prediction errors for the test set are shown in Figs. 5 and 6, from which it can be seen that the trained GSA-BP can fit the relationship of the actual gas turbine output power very well. Combining Fig. 5 and Fig. 6, the trained GSA-BP can predict the gas turbine output power well, and in the 350 sets of data used for testing, the mean square error of the prediction results reaches 0.4831, of which 15.2% of the samples have an error between 1MW-1.5MW, 41.2% of the samples have an error between 0.5MW-1MW, and the remaining 43.6% of the samples can be controlled to be within the error of 0.5MW or less.

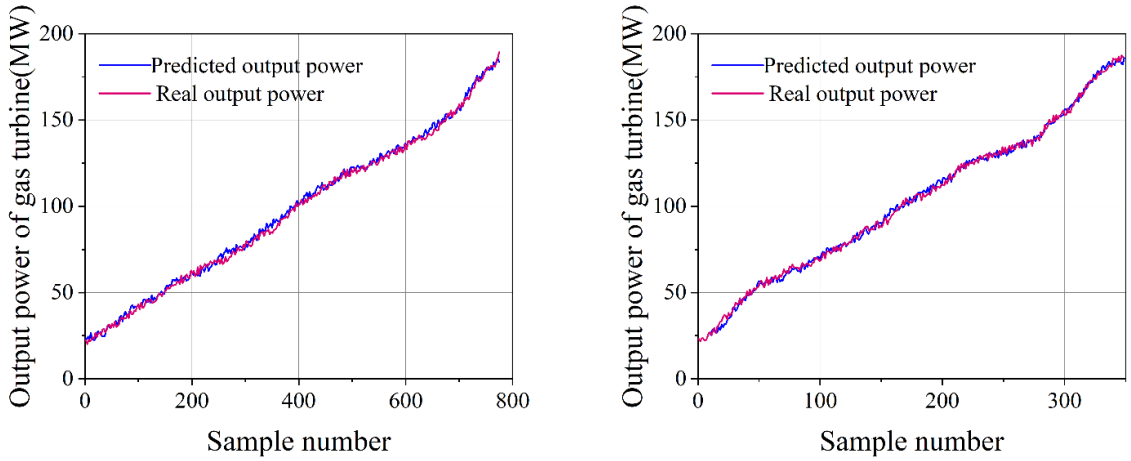

(a) Training set (b) Validation set

Figure 5: Power prediction results of gas turbine

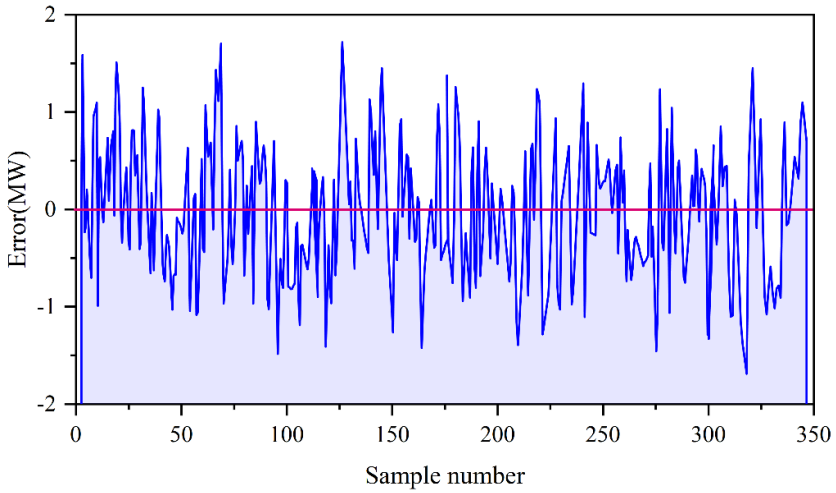

Figure 6: Power prediction error of gas turbine

The exhaust temperature of the gas turbine is shown in Figures 7 and 8, from which it can be seen that the trained GSA-BP can fit the output curve of the exhaust temperature of the gas turbine very well, and the error mean square error of the GSA-BP in predicting the output of the test samples is 0.5237, and the prediction error of only 8 of the 350 sets of operational data used for testing is more than 1.5°C, and 16.9% of the sample outputs error ranged from 1°C to 1.5°C, and the remaining 83.1% of the test samples had prediction errors of 1°C or less.

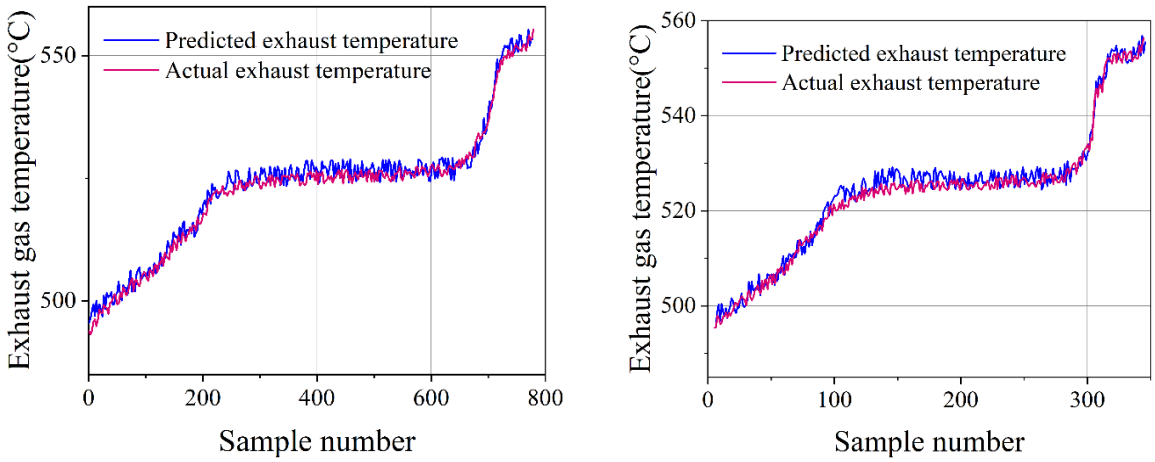

(a) Training set (b) Validation set

Figure 7: Gas turbine exhaust gas temperature prediction results

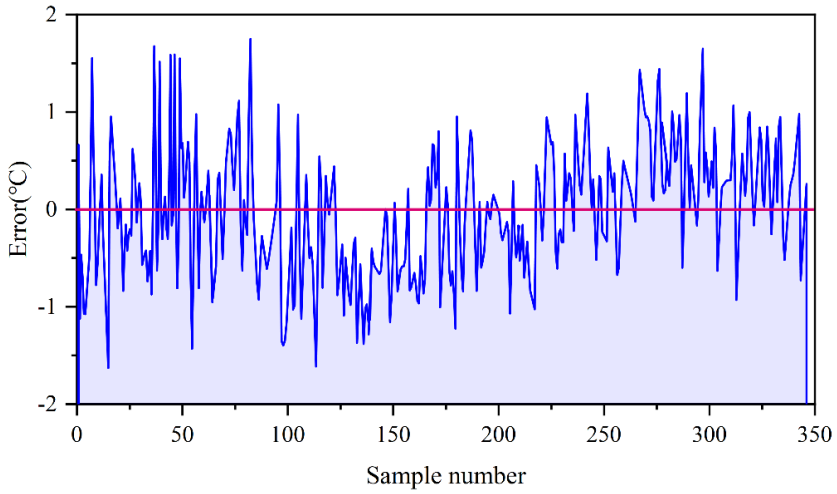

Figure 8: Gas turbine exhaust gas temperature prediction results

4 UAV-based gas unit inspection path planning

4.1 Fundamentals of the Bidirectional RRT Algorithm

The principle of random tree expansion for the bidirectional RRT algorithm is shown in Fig. 9.

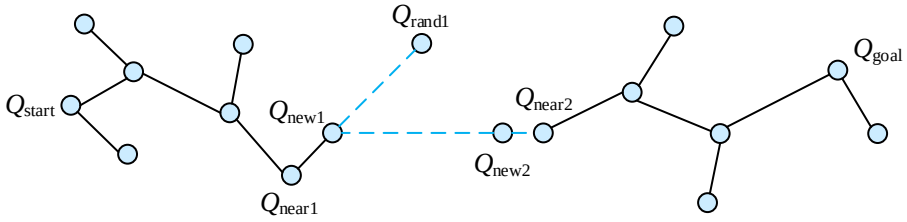

Figure 9: The Principle of Randomly Expanded Tree in Bidirectional RRT Algorithm

The bidirectional RRT algorithm takes the initial node Q_{start} as the root node of the random expansion tree, randomly selects a node Q_{start} within the accessible space, and identifies the

nearest node through a distance evaluation function, designating it as Q_{near1}. The commonly used distance evaluation functions are the Euclidean distance function and the Manhattan distance function, and the mathematical expressions of the two functions are as follows:

Euclidean distance function:

$$d = \sqrt{(X_2 - X_1) + (Y_2 - Y_1)} \tag{19}$$

Manhattan distance function:

$$d(i, j) = |X_1 - X_2| + |Y_1 - Y_2| \tag{20}$$

In this paper, we choose the Euclidean distance function, use the dotted line to connect the nodes Q_{near1} and Q_{rand}, and take $Q_{near1} \to Q_{rand}$ as the positive direction, and take Q_{near1} as the starting point to advance the unit step to form a new node Q_{new1}, and comprehensively judge whether there is an obstacle space between the two nodes, if there is no obstacle space between the two nodes, then ignore the Q_{new1} node, and conversely leave the Q_{new1} node. Repeat the above process until obtaining the maximum tolerance distance node Q_{goal} of the Euclidean distance function, and then obtain the collision-free path between the initial node Q_{start} and the maximum tolerance distance node Q_{goal} according to the backtracking method.

With Q_{start} as the initial node, once the random expansion tree identifies the node Q_{new1}, the expansion of the random tree proceeds by taking the node at the maximum tolerated distance of the Euclidean distance function as the root node of the random expansion tree. In this process, there is no need to obtain the random sampling node Q_{rand}, and it is only necessary to use the node Q_{new1} as the random sampling node Q_{rand}, and select the nearest node Q_{near2} by the distance evaluation function. Take $Q_{near2} \to Q_{new1}$ as the positive direction and Q_{near2} as the starting point to advance unit step to form a new node Q_{new2}, detect whether there is an obstacle space between the node Q_{new2} and Q_{near2}, omit Q_{new2} if there is no obstacle space, and vice versa leave Q_{new2} node. Exchange the iteration order of the random expansion tree in both directions and perform the next iteration analysis until the best path is obtained, which is the best inspection path formed by the algorithm.

4.2 Improvement of two-way RRT algorithm based on artificial potential field

4.2.1 Basic description of artificial potential fields

The fundamental concept of the artificial potential field method draws on the operating principles of naturally occurring potential fields, such as gravitational, electromagnetic, and magnetic fields. An artificial potential field is constructed within the mobile workspace of the robot, where the spatial regions occupied by obstacles are designated as repulsive potential fields, and the target destination of the robot is defined as an attractive potential field. Under the combined influence of these attractive and repulsive potential fields, the robot moves continuously through the workspace toward its goal.

The mathematical expression for the repulsive potential field acting on a node q within the workspace under the traditional artificial potential field method is:

$$P_{rep}(q)\begin{cases}\frac{1}{2}\eta\left(\frac{2}{d(q)}-\frac{1}{\rho_0}\right), & d(q)\le\rho_0\\ 0, & d(q)\le\rho_0\end{cases} \tag{21}$$

where: $P_{rep}(q)$ denotes the magnitude of the repulsive potential field; η denotes the scale factor associated with the repulsive function; ρ_0 denotes the maximum range over which the obstacle exerts repulsive influence within the workspace; and $d(q)$ refers to the shortest distance from node q to the nearest obstacle.

The mathematical expression for the gravitational potential field takes the following form:

$$P_{att}(q)=\frac{1}{2}\zeta d^2(q,q_g) \tag{22}$$

where: $P_{att}(q)$ represents the magnitude of the gravitational potential field; ζ is the scale factor of the gravitational function; and $d^2(q,q_g)$ is the shortest distance between a given node q and the destination target point of the robot.

The combined result of summing the repulsive potential field function and the gravitational potential field function yields:

$$P_{sum}(q)=P_{rep}+P_{att}(q) \tag{23}$$

The expression for the repulsive force is:

$$F_{att}(q)=-grad[P_{att}(q)]=-\zeta(q-q_g) \tag{24}$$

The expression for gravitational force is:

$$F_{rep}(q)=-grad[P_{rep}(q)]=\begin{cases}\eta\left(\frac{1}{d(q)}-\frac{1}{\rho_0}\right)\frac{1}{d^2(q)}\frac{\partial\rho}{\partial x}, & d(q)\le\rho_0\\ 0, & d(q)\le\rho_0\end{cases} \tag{25}$$

The expression for the combined repulsive and gravitational forces is:

$$F_{sum}(q)=F_{rep}(q)+F_{att}(q) \tag{26}$$

4.2.2 Bidirectional RRT Algorithm Improvement

Although there are many strengths of the bidirectional RRT algorithm compared to the basic RRT algorithm, especially in the rapid solution of problems, the bidirectional RRT algorithm, just like its predecessor, relies on random point sampling; thus, randomness and computational complexity are inevitable in its execution process. In order to improve the efficiency of the bidirectional RRT algorithm, the concept of artificial potential field is applied to the algorithm.The gravitational function $G(k)$ from the target node Q_{goal} toward the new node Q_{new} is embedded within the node determination process of the bidirectional RRT algorithm, producing a corrected new node Q_{new} that exhibits a stronger directional bias toward Q_{goal}.

With this modification, the amount of calculations and number of nodes needed to perform random sampling will decrease. When this artificial potential field is included, the gravitational force will follow a unified rule for expanding in either direction of the bidirectional RRT algorithm. The Q_{start} direction is taken here as a representative example to illustrate the changes in the process of obtaining new node Q_{new} following the introduction of the artificial potential field. Figure 10 shows the random tree expansion rule of the improved bidirectional RRT algorithm.

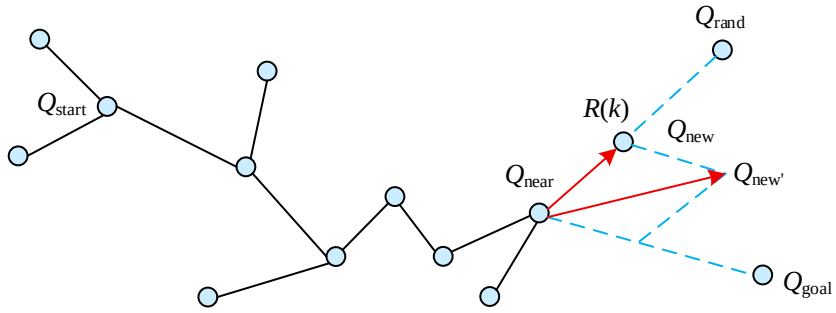

Figure 10: The Principle of Randomly Expanded Tree in the Improved Two-way RRT Algorithm

Following the incorporation of the artificial potential field concept, the starting node of the improved bidirectional RRT algorithm remains Q_{start}. Here, $R(k)$ refers to the stochastic tree growth function governing expansion from the starting node toward the new node Q_{new}, and $G(k)$ denotes the gravitational function acting from the target node Q_{goal} upon the new node Q_{new}. The positional expression of the new node under the simultaneous influence of both functions is:

$$Q_{new1}^{*} = Q_{near1} + \Delta s \left(\frac{Q_{rand1} - Q_{near1}}{\left\| Q_{rand1} - Q_{near1} \right\|} + \zeta \frac{Q_{goal} - Q_{near1}}{\left\| Q_{goal} - Q_{near1} \right\|} \right) \tag{27}$$

Similarly, with Q_{goal} as the initial node, the position expression of the new node following the introduction of the artificial potential field concept is:

$$Q_{new2}^{*} = Q_{near2} + \Delta s \left(\frac{Q_{rand2} - Q_{near2}}{\left\| Q_{rand2} - Q_{near2} \right\|} + \zeta \frac{Q_{goal} - Q_{near2}}{\left\| Q_{goal} - Q_{near2} \right\|} \right) \tag{28}$$

4.3 Gas unit inspection simulation experiment

Since the height at which UAV inspects the power line is generally maintained to be in a relatively fixed range, two-dimensional coordinates are used to describe the inspection task points. Once the path for inspecting the power line by the UAV is designed, the path will be mapped to three-dimensional space. Thus, the power line inspection problem can be converted to two-dimensional space path planning problems that avoid obstacles.

In order to examine the efficiency of the improved bidirectional RRT algorithm in performing inspection tasks, comparisons between the improved bidirectional RRT algorithm, RRT algorithm, and conventional bidirectional RRT algorithm are carried out in the power line inspection problem. In figure 11, the power line inspection environment is illustrated, wherein

the dimensions of the inspection environment are 500×500. In the above-mentioned figure, the regions colored in red refer to obstacles like trees and mountains along the power lines, and the power lines are indicated by the blue solid lines.

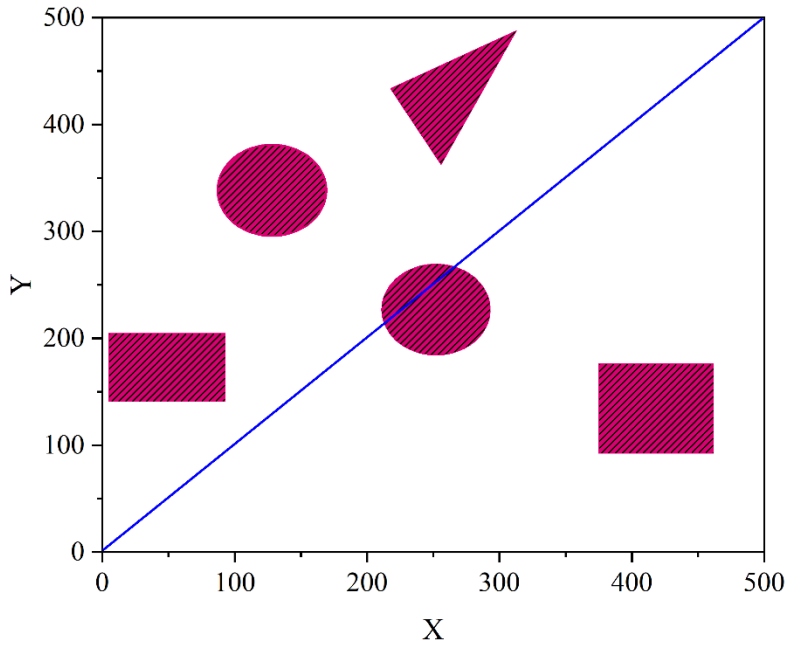

Figure 11: Environmental scenario diagram for power line inspection

In this inspection environment, the starting position of the UAV is fixed at (10,10), while that of the power lines is fixed at (490,490). The value of the step size for all the algorithms used is set to 15, and each algorithm is run 10 times independently. The result obtained from the three algorithms is depicted in Table 1, where planning time and path length are considered as two criteria in this study.

According to Table 1, the proposed bidirectional RRT algorithm performs better than the basic RRT algorithm by reducing the average path length by 38.65% and the average planning time by 4.43%. In comparison to the basic bidirectional RRT algorithm, the proposed bidirectional RRT reduces the average path length by 18.24% and average planning time by 6.09%.

In Fig. 12 below are the results on the planning process in relation to power lines inspection using the three methods as shown in (a), (b) and (c). The results in (a), (b) and (c) represent the results from the improved bidirectional RRT algorithm, bidirectional RRT algorithm and RRT algorithm respectively, but in all, the improved bidirectional RRT algorithm is faster in planning than the other two.

Table 1: Optimization results of various algorithms in power line inspection problem

Algorithm	Average planning time	Average path length
RRT algorithm	19.43	998.63
Bidirectional RRT algorithm	14.58	1016.29
Improving the bidirectional RRT algorithm	11.92	954.42

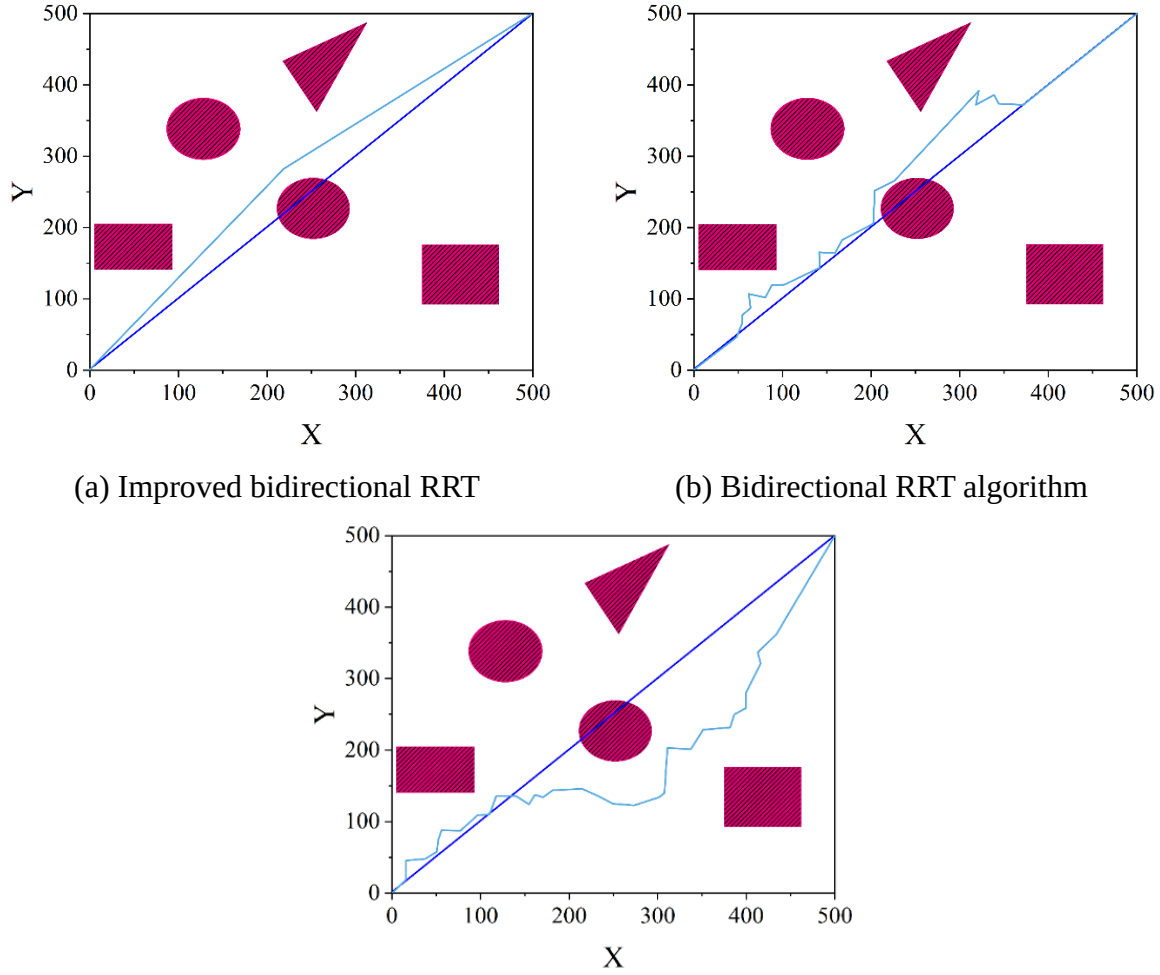

(a) Improved bidirectional RRT (b) Bidirectional RRT algorithm

(c) RRT algorithm

Figure 12: Power line inspection path diagrams using different algorithms

From the experiment results above, it can be seen that the improved bidirectional RRT algorithm performs better than the other two algorithms.

5 Gas Unit Intelligent Inspection Cockpit Platform Construction

5.1 Technical architecture

Based on the results of the research discussed in the previous section, the technical framework of the power plant cockpit platform that was developed in this paper is shown in Figure 13 below. Through the technical process of "data to model, model to application," a data mining application is created by the platform to facilitate the practical implementation of big data technology in an operational capacity.

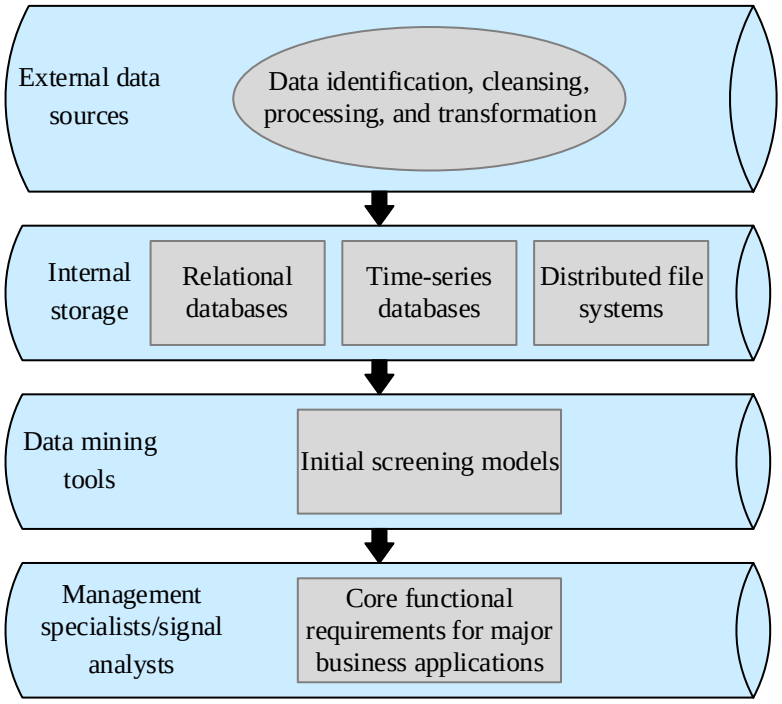

Figure 13: Platform Technology Architecture

The external data sources required by the background system of the cockpit platform are stored in the relational database, time series database and distributed file system according to the data type and application requirements after data identification, cleaning, processing and conversion; they are further analyzed by the intelligent analysis of the data mining tool, which automatically isolates the possible model structure (primary screening model) from the above massive unstructured coarse data; the primary screening model is confirmed by the The initial screening model is confirmed by the management full-time/signal analysts, thus supporting the business applications of major functional demand centers.

5.2 Functional architecture

The functional framework of the power plant cockpit platform developed in this paper is displayed in Figure 14 below and explained as follows:

Function 1: Comprehensive management of automation province and land system. Automation province and land system comprehensive management functions include: complete the interoperability of automation business data of the ground and the automation business data of the central regulator; complete the automation equipment information fusion and establish the automation equipment model library; complete the province and land comprehensive management mode, and efficiently manage each automation system in Hainan through the automation cockpit platform.

Function 2: Realize big data analysis and data label construction. This platform can analyze the quality of grid data for the characteristics of equipment quantization, diversification and complexity, and at the same time, establish a data analysis center to realize the multi-dimensional statistical analysis of equipment and assist decision-making; this platform sets up data labels for automation equipment, and incorporates big data analysis techniques in order to build a data tagging system for automation devices based on multi-dimensional features.

Function 3: Various ways of displaying alarm information. The platform can notify the duty personnel through SMS, mobile phone/tablet APP application when alarms appear, and can also display the alarm information by establishing dual modes of charts and data tables.

Function 4: Realize automated patrol. This function is first of all the automated inspection scope management, that is, by setting the content of inspection, to realize systematic management; automated inspection function can also choose the inspection result release channel, including setting SMS, system, APP and other sending channels, to inform the automated inspection status in time.

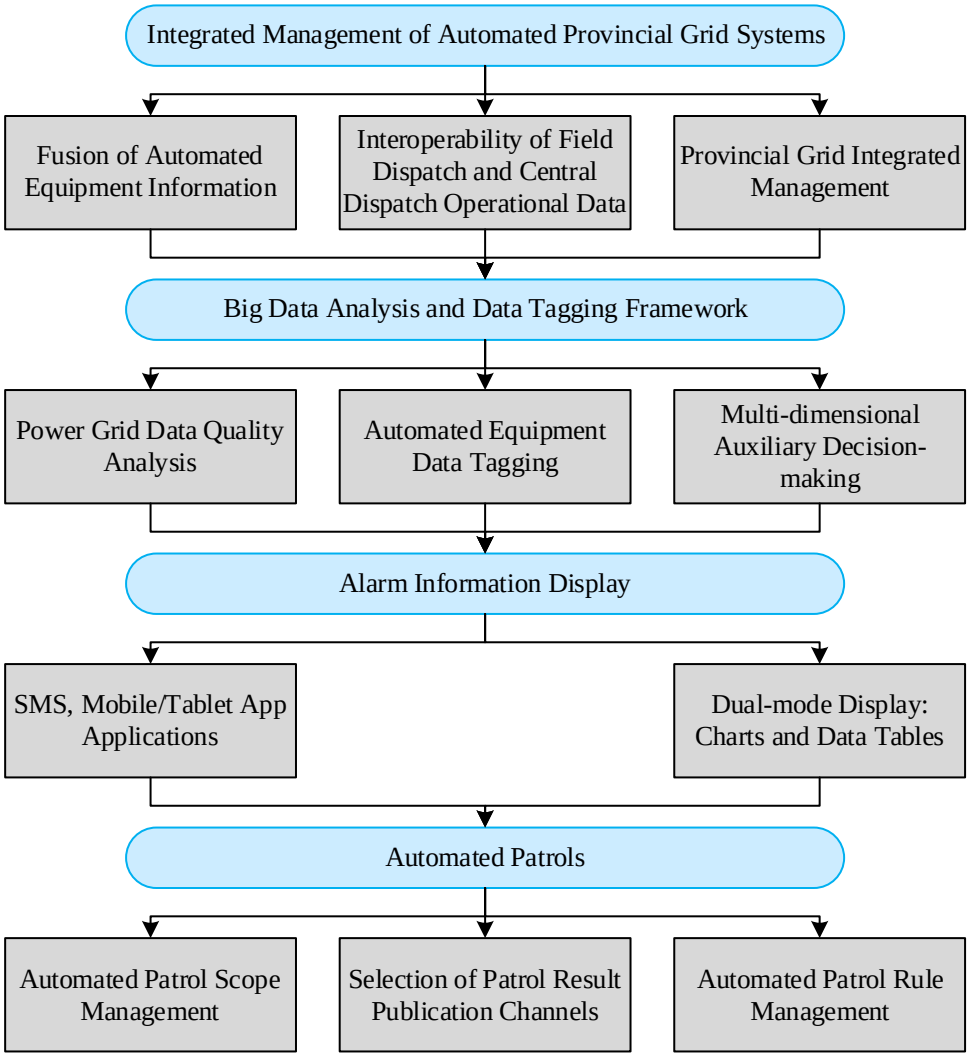

Figure 14: Platform Function Architecture

6 Conclusion

In the current paper, the gravitational search algorithm is integrated into the BP neural network, which is used to build a model for condition monitoring and prediction of gas turbine units referred to as GSA-BP. The gas turbine unit operation data of a power plant for about one year since May 27, 2021 is screened to obtain 2732 sets of valid data as the study sample. The trained GSA-BP network was tested, and the mean square error of the predicted values of gas turbine output and gas turbine exhaust temperature reached 0.4831 and 0.5237, with the maximum error not exceeding 1.5 MW and 2°C, respectively, which is of good accuracy and generalizability. The modified bidirectional RRT algorithm based on the conventional bidirectional RRT is designed by utilizing artificial potential field theory with regard to UAV inspection paths

planning of gas units. The proposed modified bidirectional RRT algorithm is tested together with the basic RRT and bidirectional RRT algorithms in the context of inspection of power lines, and the obtained results demonstrate the effectiveness of the improved bidirectional RRT algorithm.

On the basis of the research results, the gas unit intelligent inspection cockpit platform is constructed from both technical and functional aspects to realize the integration of inspection data and state visualization.

About the Author

Jiacheng Peng, was born in Anhui, China, in 1980. He received a bachelor's degree in electrical engineering from North China Electric Power University in 2004. His current research direction focuses on production technology management in gas power plants, including industrial big data analysis and industrial equipment fault diagnosis.

References

[1] Fang, J., Zeng, Q., Ai, X., Chen, Z., & Wen, J. (2017). Dynamic optimal energy flow in the integrated natural gas and electrical power systems. IEEE Transactions on Sustainable Energy, 9(1), 188-198.

[2] Safari, A., Das, N., Langhelle, O., Roy, J., & Assadi, M. (2019). Natural gas: A transition fuel for sustainable energy system transformation?. Energy Science & Engineering, 7(4), 1075-1094.

[3] He, C., Liu, T., Wu, L., & Shahidehpour, M. (2017). Robust coordination of interdependent electricity and natural gas systems in day-ahead scheduling for facilitating volatile renewable generations via power-to-gas technology. Journal of Modern Power Systems and Clean Energy, 5(3), 375-388.

[4] Mohammad, N., Mohamad Ishak, W. W., Mustapa, S. I., & Ayodele, B. V. (2021). Natural gas as a key alternative energy source in sustainable renewable energy transition: a mini review. Frontiers in Energy Research, 9, 625023.

[5] Jamróz, M., Piwowarski, M., Ziemiański, P., & Pawlak, G. (2021). Technical and economic analysis of the supercritical combined gas-steam cycle. Energies, 14(11), 2985.

[6] Ziółkowski, P., Kowalczyk, T., Lemański, M., & Badur, J. (2019). On energy, exergy, and environmental aspects of a combined gas-steam cycle for heat and power generation undergoing a process of retrofitting by steam injection. Energy Conversion and Management, 192, 374-384.

[7] Oko, C. O. C., & Njoku, I. H. (2017). Performance analysis of an integrated gas-, steam- and organic fluid-cycle thermal power plant. Energy, 122, 431-443.

[8] Pattanayak, L., & Padhi, B. N. (2021). Liquefied natural gas re-gasification cold energy hybrid system integration in gas-steam combined cycle power plant model: Enhancement in power generation and performance. Applied Thermal Engineering, 193, 116985.

[9] Xie, G., Xue, Z., Xiong, B., Huang, Y., Chen, C., Liao, Q., ... & Ma, X. (2024). Performance of Gas-Steam Combined Cycle Cogeneration Units Influenced by Heating Network Terminal Steam Parameters. Energy Engineering, 121(6).

[10] Huang, Z., Yang, C., Yang, H., & Ma, X. (2018). Ability of adjusting heating/power for combined cooling heating and power system using alternative gas turbine operation strategies in combined cycle units. Energy conversion and management, 173, 271-282.

[11] Humphrey, D. I., Barinyima, N., & Okwu, I. (2019). Effective Maintenance of Gas Turbine Power Plant to Improve Productivity. European Journal of Engineering and Technology Research, 4(4), 35-42.

[12] Udeh, G. T., & Udeh, P. O. (2019). Comparative thermo-economic analysis of multi-fuel fired gas turbine power plant. Renewable Energy, 133, 295-306.

[13] Loving, C., Mastantuono, G., Rahman, R. K., Vasu, S. S., Pigon, T., & Cloyd, S. (2025). A Comprehensive Review of Hydrogen Safety for Gas Turbine Power Plant Operations. Turbo Expo, 88803, V004T08A007.

[14] Nemitallah, M. A., Rashwan, S. S., Mansir, I. B., Abdelhafez, A. A., & Habib, M. A. (2018). Review of novel combustion techniques for clean power production in gas turbines. Energy & Fuels, 32(2), 979-1004.

[15] Haque, M. A., Nemitallah, M. A., Abdelhafez, A., Mansir, I. B., & Habib, M. A. (2020). Review of fuel/oxidizer-flexible combustion in gas turbines. Energy & Fuels, 34(9), 10459-10485.

[16] Stefanizzi, M., Capurso, T., Filomeno, G., Torresi, M., & Pascazio, G. (2021). Recent combustion strategies in gas turbines for propulsion and power generation toward a zero-emissions future: Fuels, burners, and combustion techniques. Energies, 14(20), 6694.

[17] Ibrahim, T. K., Mohammed, M. K., Al Doori, W. H. A., Al-Sammarraie, A. T., & Basrawi, F. (2019). Study of the performance of the gas turbine power plants from the simple to complex cycle: a technical review. Journal of advanced research in fluid mechanics and thermal sciences, 57(2), 228-250.

[18] Beagle, D., Moran, B., McDufford, M., & Merine, M. (2021). Heavy-Duty Gas Turbine Operating and Maintenance Considerations. GE Power Atlanta, GA.

[19] Dharmawan, D. A., & Suef, M. (2021). Optimization of Gas Turbine Component Maintenance to Improve Reliability of Power Plant Industries. IPTEK Journal of Proceedings Series, (3), 43.

[20] Hassan, M. K., Sindi, W. M., Mohamed, A., & Backar, A. H. (2024). Failure analysis of gas turbine in first stage turbine blades in an urban power plant. Journal of Engineering and Thermal Sciences, 4(1), 46-65.

[21] Matthaiou, I., Khandelwal, B., & Antoniadou, I. (2017). Vibration monitoring of gas turbine engines: Machine-learning approaches and their challenges. Frontiers in Built Environment, 3, 54.

[22] Hariyanto, B., & Romy, R. (2020). Maintenance Schedule Optimization for Turnaround Hot Gas Path Inspection of Gas Turbine in North Duri Cogeneration Plant Using Impact Method. Journal of Ocean, Mechanical and Aerospace-science and engineering-, 64(1), 25-32.

[23] Fahmi, A. T. W. K., Kashyzadeh, K. R., & Ghorbani, S. (2022). A comprehensive review on mechanical failures cause vibration in the gas turbine of combined cycle power plants. Engineering Failure Analysis, 134, 106094.

[24] Lu, R. (2020, February). Research on the structure of smart power plant based on in-depth learning. In IOP Conference Series: Earth and Environmental Science (Vol. 440, No. 3, p. 032113). IOP Publishing.